De-swirled radial inflow in a rotating cavity

P. R. Farthing* and J. M. Owen†
* Motoren- und Turbinen Union, Munchen, Germany
† School of Mechanical Engineering, University of Bath, UK

The pressure drop associated with radial inflow in a rotating cavity can be reduced by fitting de-swirl nozzles at the periphery of the system. In this work, simple theoretical models, based on solutions of the turbulent Ekman-layer equations, are used to estimate the pressure drop through both the rotating nozzles and the cavity. Although the pressure drop in the cavity itself can be reduced to virtually zero, it is shown that, when the loss in the nozzles is included, the overall pressure drop is always greater than that associated with solid-body rotation. In the main, the theoretical results are in good agreement with experimental measurements made in a rotating-cavity rig for a wide range of flow rates and rotational speeds.

Keywords: rotating cavity; rotating discs; rotating flow; de-swirled flow.

1. Introduction

Air used to cool the turbine blades and discs of a gas-turbine engine is often drawn radially inward between two corotating compressor discs, and the resulting pressure drop can approach that associated with a free vortex. Ways of reducing this pressure drop by using fins attached to one disc or by using de-swirl nozzles at the periphery of the discs have been investigated by Chew *et al.*[1] and by Farthing *et al.*[2] Although fins can reduce significantly the pressure drop, they cannot make it less than that associated with solid-body rotation and appear to be inferior to de-swirl nozzles.

De-swirl nozzles are angled to produce a tangential component of velocity of the incoming air in the opposite direction to that of the rotation of the discs. The air then enters the system with a lower angular velocity than that of the discs, and the resulting pressure drop can be reduced. In fact, Farthing *et al.* showed that, by swirling the air so that it actually rotated in the opposite direction to the discs, the pressure drop in the cavity could be reduced virtually to zero.

Farthing *et al.* obtained numerical solutions of the momentum-integral equations, which predicted with good accuracy the resulting pressure distribution inside the cavity. However, neither their theoretical model nor their experimental results took account of the pressure drop in the de-swirl nozzles themselves. It is the object of this work to produce a simple analytical model that can predict the resulting pressure drop in both the nozzles and the cavity.

The theoretical model and experimental apparatus are described in Sections 2 and 3, respectively, and the results are presented in Section 4.

2. Calculation of the pressure drop

The overall pressure drop in the system consists of the drop through the de-swirl nozzles and the drop in the cavity itself. It is convenient to separate these two effects.

Address reprint requests to Professor Owen at the School of Mechanical Engineering, University of Bath, Claverton Down, Bath, BA2 7AY, UK.

Received 22 January 1990; accepted 13 August 1990

2.1 Pressure drop in the cavity

Owen *et al.*[3] obtained solutions of the momentum-integral equations for laminar and turbulent source-sink flow in a rotating cavity (based on 1/7th power laws for the turbulent case). If the equations are expressed in a rotating frame of reference and if the angular speed of the fluid is sufficiently close to that of the discs, the nonlinear inertia terms can be neglected by comparison with the Coriolis terms. We refer to the resulting equations as the "linear equations" (see Section 2.1.1) and the full equations as the "nonlinear equations" (see Section 2.1.2). The linear model is based on the linear equations; the nonlinear model is based on an improved approximation of Owen[4] (which is discussed further by Owen and Rogers[5]). As the speed of the fluid approaches that of the disc, the "linear solution" is obtained; as the speed of the fluid tends to zero, the "free-disc solution" of von Karman[6] is retrieved.

For the radial inflow case considered here, the flow depends on the Reynolds number ($\mathrm{Re}_\phi = \Omega b^2/\nu$), the nondimensional flow rate ($C_w = Q/\nu b$), and the radius ratio ($x_a = a/b$). It also depends on the inlet swirl fraction c, which is defined as the ratio of the tangential speed of the fluid at inlet to that of the cavity at $r = b$. Using the linear equations, it was shown by Owen *et al.* that, for turbulent flow, a single nondimensional variable ($\lambda_T = C_w/\mathrm{Re}_\phi^{0.8}$) could be used to replace C_w and Re_ϕ. (The undefined variables used here and elsewhere in this article are included in the Notation.)

Firouzian *et al.*[7] carried out a combined theoretical and experimental study of radial inflow in a rotating cavity and confirmed that the nondimensional pressure drop depended on λ_T, c, and x_a. Their experiments were conducted in a rotating cavity, with a gap ratio ($G = s/b$) of 0.133 and a radius ratio of $x_a = 0.1$, for a range of C_w and Re_ϕ. The measured velocities and pressure drops mainly were in good agreement with results obtained from the linear equations.

2.1.1 Linear model. Figure 1 shows that the flow structure includes a source region, Ekman layers on each disc, an inviscid core between the Ekman layers, and a sink layer at the center of the cavity. In the source region, free-vortex flow occurs such that

$$\frac{\bar{V}_\phi}{\Omega r} = cx^{-2} \tag{2.1}$$

where c is the swirl fraction of the fluid entering the cavity and

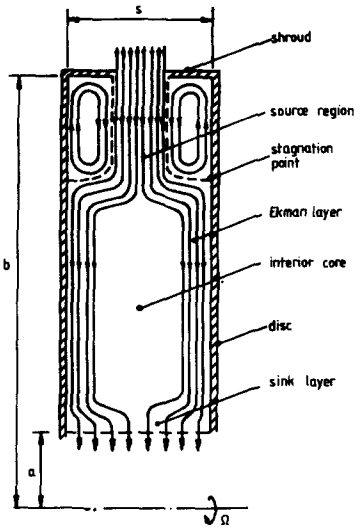

Figure 1 Schematic diagram of flow structure in a rotating cavity with radial inflow

the overbar is used denote conditions outside the boundary layers. In the core, Owen *et al.*[3] showed that, for turbulent flow, the linear Ekman-layer equations can be solved to give

$$\frac{\bar{V}_\phi}{\Omega r} = 1 - \mathrm{sgn}(Q) 2.22 |\lambda_T|^{5/8} x^{-13/8} \tag{2.2}$$

and the edge of the source region, where $x = x_e$, is given by

$$x_e = (c - 2.22|\lambda_T|^{5/8} x_e^{3/8})^{1/2} \tag{2.3}$$

By convention, Q and λ_T are taken to be positive for radial outflow and negative for inflow. It should also be noted that Equation 2.2 implies that $\bar{V}_\phi/\Omega r$ is less than or greater than unity if Q is positive or negative, respectively.

The radial pressure gradient can be calculated from

$$\frac{1}{\rho}\frac{dp}{dr} = \frac{\bar{V}_\phi^2}{r} \tag{2.4}$$

and the pressure coefficient for the cavity, $C_{p,c}$, is found from

$$C_{p,c} = 2\int_{x_a}^{1} x\left(\frac{\bar{V}_\phi}{\Omega r}\right)^2 dx \tag{2.5}$$

As the sink layer is small, Equation 2.5 can be evaluated using Equations 2.1 and 2.2 to give

$$C_{p,c} = (x_e^2 - x_a^2) + c^2(x_e^{-2} - 1) + 23.7|\lambda_T|^{5/8}(x_e^{3/8} - x_a^{3/8}) + 7.89|\lambda_T|^{5/4}(x_a^{-5/4} - x_e^{-5/4}) \tag{2.6}$$

Equation 2.6 is only valid for $x_e \geq x_a$ (where the source region does not fill the entire cavity). At large flow rates, where the source region does fill the cavity, free vortex flow is assumed to occur throughout, such that

$$C_{p,c} = c^2(x_a^{-2} - 1) \tag{2.7}$$

which is equivalent to setting $x_e = x_a$ in Equation 2.6. Another

Notation

a	Inner radius of cavity
b	Outer radius of cavity
c	Inlet swirl fraction, $V_{\phi I}/\Omega b$
c_{eff}	Effective swirl fraction
C_d	Coefficient of discharge
C_p	Local pressure coefficient, $\Delta p/\frac{1}{2}\rho\Omega^2 b^2$
$C_{p,c}$	Pressure coefficient for cavity, $\Delta p_c/\frac{1}{2}\rho\Omega^2 b^2$
$C_{p,n}$	Pressure coefficient for nozzles, $\Delta p_n/\frac{1}{2}\rho\Omega^2 b^2$
$C_{p,T}$	Overall pressure coefficient, $C_{p,c} + C_{p,n}$
C_w	Nondimensional flow rate, $Q/\nu b$
d	Outlet diameter of de-swirl nozzles
f	Function of β
g	Function of β
G	Gap ratio of cavity, s/b
i, j, k	Unit vectors (cartesian coordinates)
$\dot{m}$	Mass flow rate
M	Frictional moment exerted by the shroud on the fluid
N	Number of de-swirl nozzles
p	Static pressure
P	Reduced pressure, $p - \frac{1}{2}\rho\Omega^2 r^2$
q	Magnitude of velocity in the nozzles
Q	Volumetric flow rate
r	Radial coordinate
Re_ϕ	Rotational Reynolds number, $\Omega b^2/\nu$
s	Axial distance between discs
V_ϕ	Tangential component of velocity (in a stationary frame)
x	Nondimensional radial coordinate, r/b
X	Position vector in rotating frame of reference, $X\mathbf{i} + Y\mathbf{j} + Z\mathbf{k}$
x_a	Ratio of inner-to-outer radii of cavity, a/b
X, Y, Z	Cartesian coordinates
u	Velocity in rotating frame of reference, $u\mathbf{i} + v\mathbf{j} + w\mathbf{k}$

Greek symbols

γ_0	Function of β
β	Relative rotational speed of the core, $\bar{V}_\phi/\Omega r$
Δp	Local pressure difference between $x = 1$ and local value of x
Δp_c	Pressure difference between $x = 1$ and $x = 0.5$
Δp_n	Pressure difference across the de-swirl nozzles
α_0	Function of β
θ	Angle of nozzles to tangential direction
λ_T	Turbulent flow parameter, $C_w/\mathrm{Re}_\phi^{0.8}$
ν	Kinematic viscosity
ρ	Density
τ_ϕ	Tangential component of shear stress on disc at $x = 1$
ω	Vorticity in rotating frame of reference
Ω	Angular speed of cavity
$^i\mathbf{\Omega} = \Omega\mathbf{k}$	Angular velocity of discs and nozzles

Subscripts

a	Refers to conditions at $r = a$
e	Edge of source region
ent	Refers to entrainment
I	Refers to inlet
o	Refers to outlet
ϕ	Refers to tangential direction
1, 2	Refers to inlet and outlet of nozzles

Other

An overbar is used to refer to values in the core outside the boundary layers.

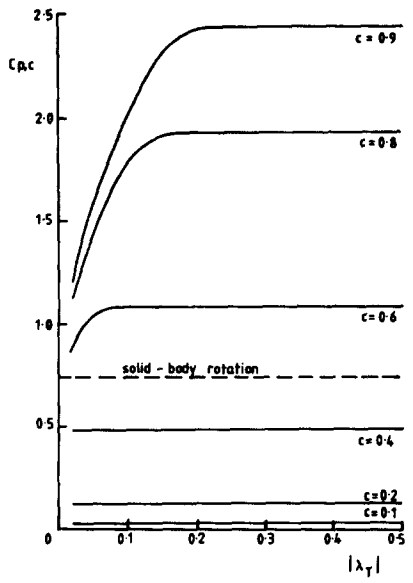

Figure 2 Effect of c on variation of $C_{p,c}$ with $|\lambda_T|$ for $x_a = 0.5$ (linear solution, no mixing)

important case is that of solid-body rotation, where $\bar{V}_\phi/\Omega r = 1$ and Equation 2.5 can be integrated to give

$$C_{p,c} = 1 - x_a^2 \tag{2.8}$$

The variation of $C_{p,c}$ with $|\lambda_T|$ according to Equation 2.6 is shown in Figure 2 for the case where $x_a = 0.5$, which corresponds to the radius ratio of the experimental rig described in Section 3. For the larger values of $|\lambda_T|$, $C_{p,c}$ tends to the limit given by Equation 2.7, and Equation 2.8 is included as a convenient datum.

2.1.2 Nonlinear model. As outlined, an improved approximation for $\bar{V}_\phi/\Omega r$ in the core region was found by Owen,[4] where

$$\beta(x) = \frac{\bar{V}_\phi}{\Omega r} = 1 - \mathrm{sgn}(Q)\left(\frac{30}{49\pi\alpha_o(\beta)\gamma_o(\beta)}\right)^{5/8} |\lambda_T|^{5/8} x^{-13/8} \tag{2.9}$$

$$\alpha_o(\beta) = 0.162(1+8\beta)^{1/2}(1-0.229\beta)^{-1/2} \tag{2.10}$$

$$\gamma_o(\beta) = 0.526(1-0.019\beta)^{0.3}(1-0.229\beta)^{0.1}(1+8\beta)^{-0.4} \times (1+1.608\beta)^{-0.8} \tag{2.11}$$

For $\beta \simeq 1$ (which corresponds to the linear case), Equation 2.9 reduces to Equation 2.2; $\beta = 0$ corresponds to the so-called free-disc case.

The pressure coefficient can be evaluated numerically from Equations 2.1, 2.5, and 2.9 to give

$$C_{p,c} = c^2(x_e^{-2} - 1) + 2\int_{x_a}^{x_e} x\beta^2(x)\,dx \tag{2.12}$$

where x_e is the value of x at which $\bar{V}_\phi/\Omega r$ calculated from Equation 2.1 equals that calculated from Equation 2.9. (For the case where $\beta(x) \leqslant 0$, the values of $\alpha_o(0)$ and $\gamma_o(0)$ are used in Equation 2.9.)

2.1.3 Effective swirl fraction. The pressure coefficient can only be evaluated if the swirl fraction is known. In practice, although knowledge of the angle of the de-swirl nozzles enables the *inlet* swirl fraction, c, to be determined *a priori*, mixing between the incoming flow and that in the cavity means that the *effective* swirl fraction, c_{eff}, is not, in general, equal to c.

It was stated in Section 2.1.1 that $\bar{V}_\phi/\Omega r$ is less than unity when Q is positive; this implies that there is radial outflow in the boundary layers in the source region wherever $\bar{V}_\phi/\Omega r < 1$. This radial outflow mixes with the inflow from the de-swirl nozzles, thereby altering the swirl fraction of the incoming flow. This is shown schematically in Figure 3, where $\dot{m}_I$ refers to the mass flow rate at inlet to the cavity and $\dot{m}_{\mathrm{ent}}$ to that inside the boundary layer at $r = b$. It is assumed that (i) the mixing occurs in a thin layer (such that $r \simeq b$ at the inner edge of the layer); (ii) the frictional moment exerted by the shroud, M, equals the rate of change of angular momentum of the fluid passing through the mixing layer; and (iii) the shear stress on the shroud, τ_ϕ, equals that on the disc at $r = b$. Using these assumptions it follows that

$$M = (|\dot{m}_I| + 2\dot{m}_{\mathrm{ent}})\bar{V}_{\phi,o}b - (2\dot{m}_{\mathrm{ent}}V_{\phi,\mathrm{ent}} + |\dot{m}_I|V_{\phi,I})b \tag{2.13}$$

where the subscript I refers to conditions at the inlet to the control volume, o to conditions at the outlet, and ent to the fluid entrained by the boundary layers on the disc.

The results of Owen[4] give

$$\frac{\dot{m}_{\mathrm{ent}}}{\mu b} = f(\beta)\mathrm{Re}_\phi^{4/5} \tag{2.14}$$

$$\frac{\tau_\phi}{\rho\Omega^2 b^2} = -g(\beta)\mathrm{Re}_\phi^{-1/5} \tag{2.15}$$

and

$$\frac{V_{\phi,\mathrm{ent}}}{\Omega b} = \frac{1}{6} + \frac{5}{6}\beta \tag{2.16}$$

where

$$f(\beta) = \mathrm{sgn}(1-\beta)2.566\alpha_o(\beta)\gamma_o(\beta)|1-\beta|^{8/5} \tag{2.17}$$

and

$$g(\beta) = \mathrm{sgn}(1-\beta)0.0225[1+\alpha_o^2(\beta)]^{3/8}\gamma_o(\beta)^{-1/4}|1-\beta|^{8/5} \tag{2.18}$$

with $\alpha_o(\beta)$ and $\gamma_o(\beta)$ being given by Equations 2.10 and 2.11 and β by Equation 2.9.

The moment on the shroud is

$$M = -2\pi b^2 s\tau_\phi \tag{2.19}$$

The inlet swirl fraction is

$$c = \frac{V_{\phi,I}}{\Omega b} \tag{2.20}$$

and the outlet swirl fraction, c_{eff}, is equal to β.

Hence Equation 2.13 can be rewritten as

$$c_{\mathrm{eff}} = \frac{c + \frac{1}{3}f(\beta)|\lambda_T^{-1}| + 2\pi g(\beta)G|\lambda_T^{-1}|}{1 + \frac{1}{3}f(\beta)|\lambda_T^{-1}|} \tag{2.21}$$

(For the case where $\beta \leqslant 0$, the values for $f(\beta)$ and $g(\beta)$ with $\beta = 0$ were used in Equation 2.21 to calculate c_{eff}.)

The variation of c_{eff} with $|\lambda_T|$ according to Equation 2.21 is shown in Figure 4 for $-0.4 \leqslant c \leqslant 0.9$ and $G = 0.267$. It can be

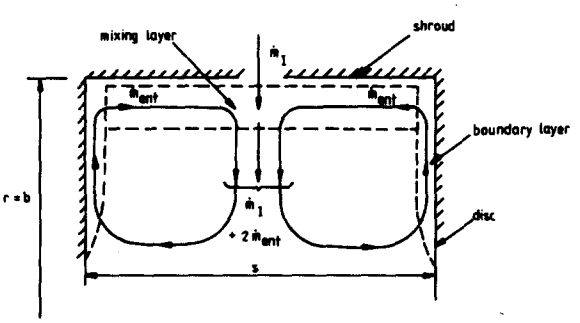

Figure 3 Mixing layer in source region

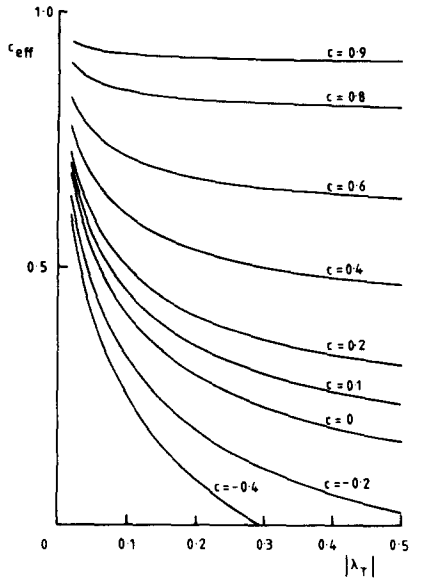

Figure 4 Effect of c on variation of c_{eff} with $|\lambda_T|$ for $x_s=0.5$

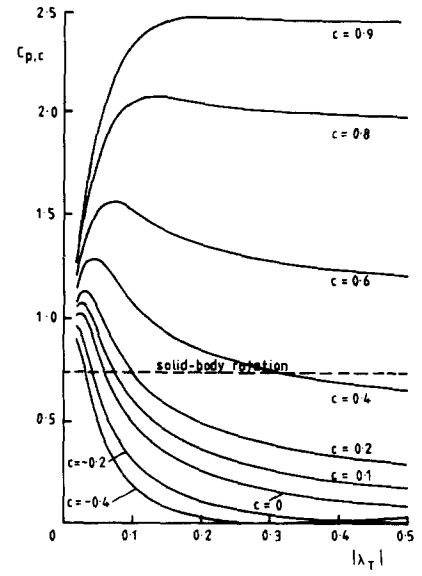

Figure 5 Effect of c on variation of $C_{p,c}$ with $|\lambda_T|$ for $x_s=0.5$ (nonlinear solution, with mixing)

seen that $c_{eff}>c$, that $c_{eff}\to 1$ as $|\lambda_T|\to 0$, and that $c_{eff}\to c$ as $|\lambda_T|\to\infty$. The variation of c_{eff} with $|\lambda_T|$ is more pronounced at the small values of c.

The variation of $C_{p,c}$ with $|\lambda_T|$, according to the nonlinear solution and with c replaced by c_{eff}, is shown in Figure 5; it should be noted that similar results were obtained using Equation 2.6, the linear solution, with c replaced by c_{eff}. Comparison with Figure 2 reveals that the mixing process has the greatest effect on $C_{p,c}$ at the smallest values of c. For small values of $|\lambda_T|$, where c_{eff} can be much greater than c, the pressure coefficients shown in Figure 5 are significantly greater than those in Figure 2, and a turning point in each curve can be clearly seen. It is also interesting to note that $C_{p,c}$ can be reduced to zero; for example, $C_{p,c}=0$ at $|\lambda_T|\simeq 0.3$ when $c=-0.4$. As shown in Figure 4, those conditions correspond to $c_{eff}=0$: The negative swirl of the incoming fluid is neutralized by the mixing process, resulting in a negligible pressure drop in the cavity.

The pressure drop in the nozzles, which has so far been ignored, is now considered.

2.2 Pressure drop across a rotating nozzle

Figure 6 shows the coordinate system used for flow through a nozzle rotating with constant angular velocity $\mathbf{\Omega}=\Omega\mathbf{k}$. For steady, incompressible inviscid flow in a coordinate system rotating with angular velocity $\mathbf{\Omega}$ and in which gravitational effects are negligible, the equation of motion (see Batchelor[8]) is

$$\mathbf{u}\times(\boldsymbol{\omega}+2\mathbf{\Omega})=-\nabla\left[\tfrac{1}{2}q^2+\frac{p}{\rho}-\tfrac{1}{2}(\mathbf{\Omega}\times\mathbf{X})^2\right] \tag{2.22}$$

where

$$\mathbf{X}=X\mathbf{i}+Y\mathbf{j}+Z\mathbf{k}$$

$$\mathbf{u}=u\mathbf{i}+v\mathbf{j}+w\mathbf{k}$$

$$q^2=\mathbf{u}\cdot\mathbf{u}$$

and $\boldsymbol{\omega}$ is the vorticity.

If Equation 2.22 is integrated in the direction of the velocity vector, then the Coriolis and vorticity terms are identically zero and

$$\tfrac{1}{2}q^2+\frac{p}{\rho}-\tfrac{1}{2}(\mathbf{\Omega}\times\mathbf{X})^2=\text{constant} \tag{2.23}$$

Applying Equation 2.23 to flow through the rotating nozzle from $r=r_1$ to $r=r_2$ (where $r^2=X^2+Y^2$), it follows that

$$\tfrac{1}{2}q_1^2+\frac{p_1}{\rho}-\tfrac{1}{2}\Omega^2r_1^2=\tfrac{1}{2}q_2^2+\frac{p_2}{\rho}-\tfrac{1}{2}\Omega^2r_2^2 \tag{2.24}$$

If the flow starts in a large "reservoir" such that $q_1=0$ (which is a good approximation for the present system) then

$$q_2=\left[\frac{2(P_1-P_2)}{\rho}\right]^{1/2} \tag{2.25}$$

where $P=p-\frac{1}{2}\rho\Omega^2r^2$ is the reduced pressure.

To account for viscous effects, it is convenient to introduce a discharge coefficient, C_d, such that

$$C_d=\frac{q_2}{[2(P_1-P_2)/\rho]^{1/2}} \tag{2.26}$$

The pressure drop can be expressed in terms of the swirl fraction, c, where

$$c=\frac{\Omega r_2-q_2\cos\theta}{\Omega r_2} \tag{2.27}$$

Hence Equation 2.26 can be written as

$$\frac{P_1-P_2}{\frac{1}{2}\rho\Omega^2r_2^2}=\left(\frac{1-c}{C_d\cos\theta}\right)^2 \tag{2.28}$$

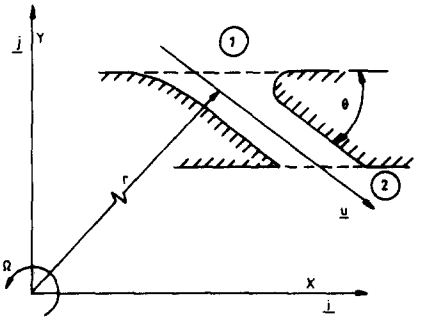

Figure 6 Coordinate system for nozzles

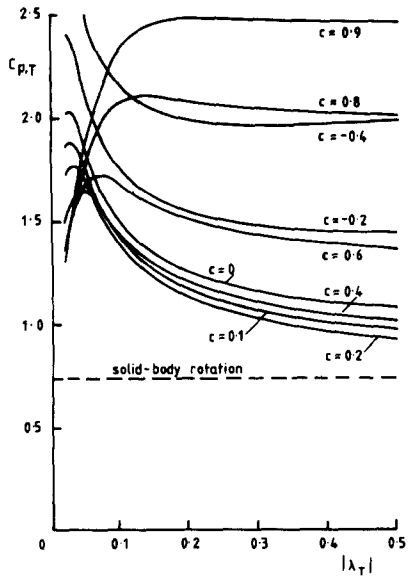

Figure 7 Effect of c on variation of $C_{p,T}$ with $|\lambda_T|$ for $x_a=0.5$ (nonlinear solution and "ideal nozzles")

Alternatively, the static-pressure drop can be presented in terms of a pressure coefficient for the nozzles, $C_{p,n}$, defined as

$$C_{p,n}=\frac{p_1-p_2}{\frac{1}{2}\rho\Omega^2 r_2^2} \tag{2.29}$$

Using Equation 2.28, it follows that

$$C_{p,n}=\left(\frac{1-c}{C_d\cos\theta}\right)^2+\left(\frac{r_1}{r_2}\right)^2-1 \tag{2.30}$$

The "ideal nozzle" would be one for which $C_d=1$, $r_1=r_2$, and $\theta=0$. Under these conditions

$$C_{p,n}=(1-c)^2 \tag{2.31}$$

This is the minimum pressure drop that can occur across the nozzles.

2.3 Overall pressure drop

The overall pressure coefficient, $C_{p,T}$, for the nozzles and the cavity can be obtained by adding the appropriate values of $C_{p,n}$ and $C_{p,c}$. To illustrate this, Figure 7 shows the variation of $C_{p,T}$ with $|\lambda_T|$ for the case of "ideal nozzles."

Comparing Figures 5 and 7, we see that the effect of the nozzles is much greater at the smaller values of c. For example, at $|\lambda_T|=0.3$ and $c=-0.4$, $C_{p,c}\simeq 0$ (Figure 5), whereas $C_{p,T}\simeq 2$ (Figure 7). In fact, for this value of $|\lambda_T|$, Figure 7 shows that a value of $c=+0.2$ produces the smallest value of $C_{p,T}$; however, even this value of $C_{p,T}$ is greater than that associated with solid-body rotation.

The optimum value of c for any system will depend on $|\lambda_T|$, x_a, and the nozzle geometry. In principle, this optimum value of c and the minimum value of $C_{p,T}$ can be estimated using Equations 2.21, 2.12, and 2.30.

3. Experimental apparatus

Details of the apparatus and instrumentation are given by Farthing[9] and Farthing *et al.*,[2] but for completeness the main features are described as follows.

Simplified diagrams of the rig and the de-swirl nozzles are shown in Figure 8. The discs had an outer radius of 381 mm and an axial spacing 102 mm, and the shroud contained 30 holes, which were covered with porous foam to ensure solid-body rotation of the air entering the system. The de-swirl nozzles were machined from a ring of Rohacell plastic foam, and 60 equally spaced holes were drilled at an angle of $\theta=30°$ to the tangential direction at each of the three axial locations

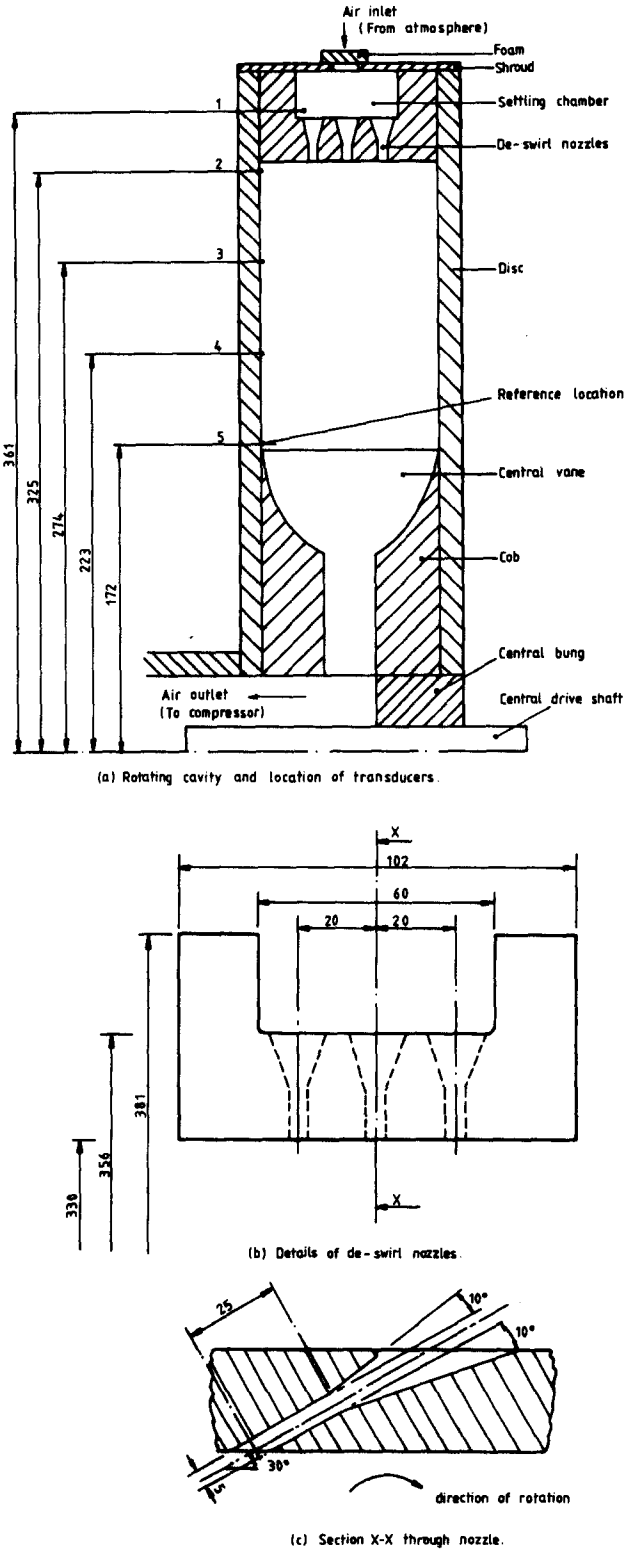

Figure 8 Schematic diagram of rotating cavity used in experiments

shown. The outer radius of the cavity was taken to be the inner radius of the nozzle ring where $r=b=330$ mm, and the outlet diameter of the nozzles, d, was 5 mm.

The inlet swirl fraction, c, is given by

$$c=1-\frac{4\cos\theta}{\pi N}\left(\frac{b}{d}\right)^2\frac{|C_w|}{\mathrm{Re}_\phi}=1-\frac{4\cos\theta}{\pi N}\left(\frac{b}{d}\right)^2\frac{|\lambda_T|}{\mathrm{Re}_\phi^{0.2}} \qquad (3.1)$$

where N is the number of nozzles. For the experiments, N was varied by inserting rubber bungs in some of the 180 nozzles.

The discs could be rotated up to 2,000 rev/min by means of a variable-speed electric motor, and flow rates up to 0.1 kg/s of air were achieved by a centrifugal compressor. To minimize the overall pressure drop, radial vanes were installed at the center of the cavity. The vanes, and the cobs (or bulbous hubs) shown in Figure 8, were downstream of the test section and played no part in the experiments reported here.

Pressure taps were located on one of the discs at radial locations of $r=172$, 223, 274, 325, and 361 mm. Kulite differential-pressure transducers were inserted in the four outer taps (numbers 1–4), and the innermost tap (number 5) was used as a datum from which the other pressures could be measured. Signals were brought out through instrumentation slip rings, and the voltages were measured by a Solatron data logger.

The rotational speed of the discs was measured to an accuracy of ± 1 rev/min by means of a magnetic transducer and electronic timer, and the flow rate of air was measured to an accuracy of $\pm 3\%$ by differential-pressure meters. Corrections to the flow rate, because of leakage through seals, and to the pressure measurements are described in References 2 and 9.

4. Comparison between calculated and measured pressure drops

Figure 9 shows the variation of the local pressure coefficient, C_p, with the nondimensional radius, x, for $\mathrm{Re}_\phi=1.21\times10^6$ and $N=40$ (see Equation 3.1). Agreement between the measured values and those calculated from the nonlinear theory is reasonable.

In the experiments, the pressure drop was the dependent variable; λ_T and c were varied in a controlled fashion, and the resulting pressures were measured. In a gas-turbine engine, the pressure drop between the compressor bleedoff and, for example,

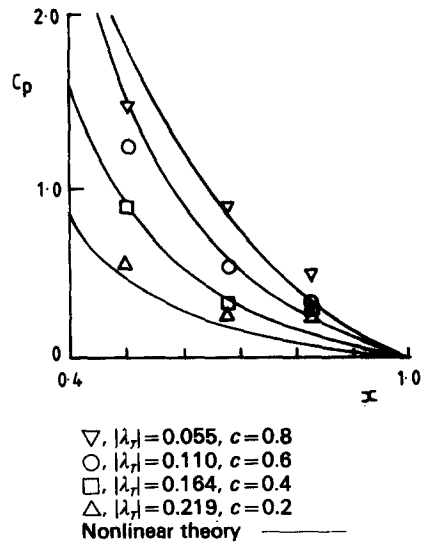

Figure 9 Effect of c on variation of C_p with x for $\mathrm{Re}_\phi\times1.21\times10^6$

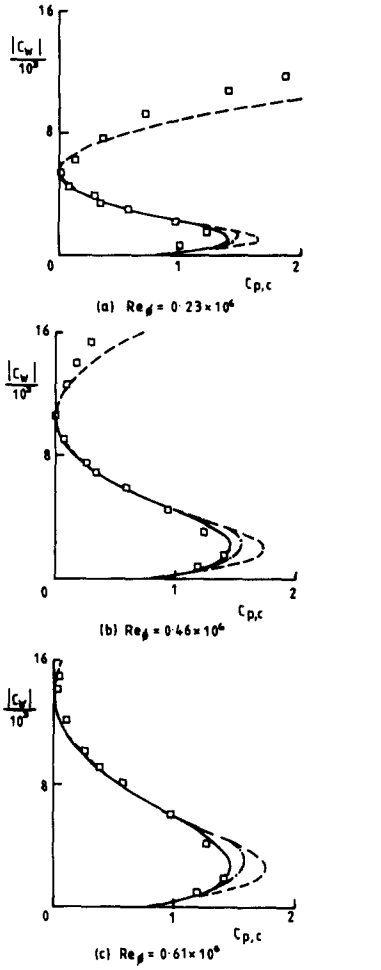

Figure 10 Effect of Re_ϕ on variation of $|C_w|$ with $C_{p,c}$

the turbine blades is fixed; the flow rate of cooling air is determined by the available pressure difference. It is useful therefore to plot the variation of $|C_w|$ with $C_{p,c}$, as shown in Figure 10. For the experimental data (where $N=80$), as $|C_w|$ increases, c decreases in the manner given by Equation 3.1.

Figure 10a shows the variation of $|C_w|$ with $C_{p,c}$ for $\mathrm{Re}_\phi=0.23\times10^6$. The resulting "$s$ curve" shows that there are up to three values of $|C_w|$ for each value of $C_{p,c}$! This can be explained by considering Figure 5: The turning points at $|C_w|\simeq10^3$ and 5×10^3 correspond to the maximum and minimum values of $C_{p,c}$, respectively. The latter case corresponds to $C_{p,c}\simeq0$ and $c_{\mathrm{eff}}\simeq0$; for $C_w\gtrsim5\times10^3$, $c_{\mathrm{eff}}<0$, and the pressure coefficient increases as the tangential velocity of the fluid (which is now rotating in the opposite direction to that of discs) increases with increasing $|C_w|$. Similar results are shown in Figure 10b and 10c for $\mathrm{Re}_\phi=0.46\times10^6$ and 0.61×10^6. It should be emphasized that, as previously stated, the experimental data were obtained by fixing λ_T and c; the pressure drop was the dependent variable in the experiment, *not* the independent variable, as implied by Figure 10. (If the pressure drop were to be the independent variable, as is the case in an engine, "jump phenomena" between the higher and lower $|C_w|$ curves would be expected to occur, causing associated hysteresis effects.)

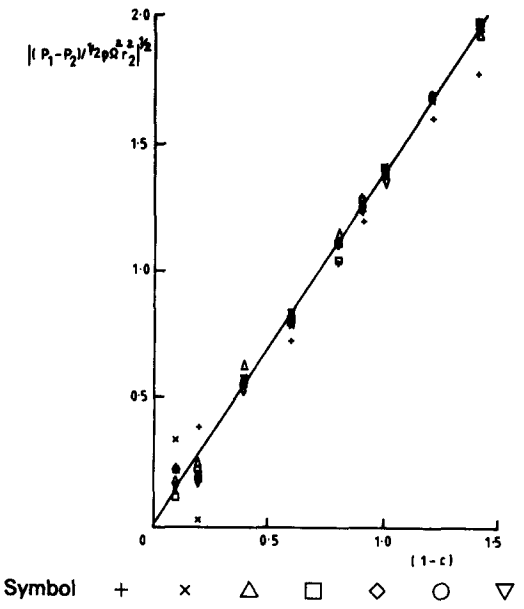

Figure 11 Experimentally measured variation of $[(P_1-P_2)/\frac{1}{2}\rho\Omega^2 r_2^2]^{1/2}$ with $(1-c)$

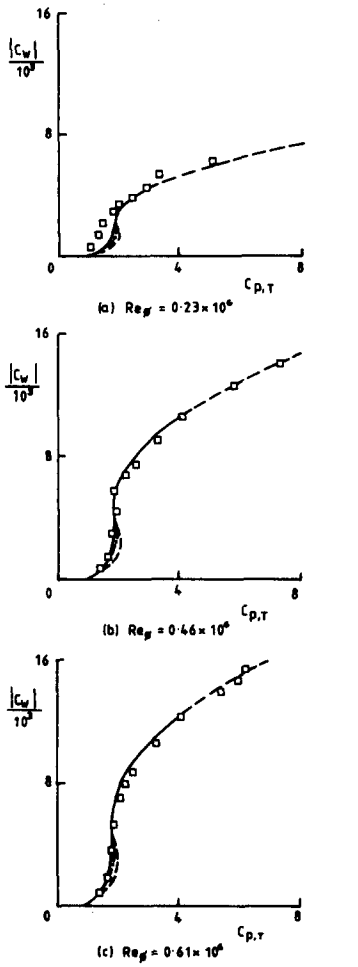

Figure 12 Effect of Re$_\phi$ on variation of $|C_w|$ with $C_{p,T}$

The three curves shown in Figure 10 correspond to the numerical solution of the momentum-integral equations according to Farthing *et al.*[2] and to the linear and nonlinear solutions (Equations 2.6 and 2.12, respectively) with c replaced by c_{eff}; no integral solutions were obtained for $c_{\text{eff}}<0$. It can be seen that, although the integral equations provide the closest fit to the experimental data, the two approximate solutions are both reasonable, except near the turning point at the smaller values of $|C_w|$. (The reason why, at the lower value of $|C_w|$, the linear model is marginally superior to the nonlinear one is not known; presumably, the errors associated with the various assumptions interact more favourably in the linear model.)

Figure 11 shows the variation of the nondimensional pressure drop through the nozzles with $1-c$. According to Equation 2.28,

$$C_d=\frac{1-c}{\cos\theta\,[(P_1-P_2)/\frac{1}{2}\rho\Omega^2 r_2^2]^{1/2}} \tag{4.1}$$

and Figure 11 confirms that most of the experimental data lie close to a straight line. For the nozzle geometry used in the experiments ($\theta=30°$, $r_2=330$ mm), the gradient of the line suggests that $C_d\simeq 0.82$.

Figure 12 shows the variation of $|C_w|$ with $C_{p,T}$ for Re$_\phi/10^6=$ 0.23, 0.46, and 0.61. The theoretical curves were calculated by adding $C_{p,n}$ (obtained from Equation 2.30 with $C_d=0.82$) to the appropriate value of $C_{p,c}$. Comparison of Figures 10 and 12 shows that the nozzles not only increase significantly the overall pressure drop (which is always greater than that associated with solid-body rotation, as was also shown for the "ideal nozzles" in Figure 7), but they also tend to make the "s curve" monotonic. The approximate solutions provide a good fit to most of the experimental data and should prove useful for design purposes.

5. Conclusions

This work, which studies the use of de-swirl nozzles to reduce the pressure drop in a rotating cavity with radial inflow, is an extension of the work of Farthing *et al.*[2] Whereas the latter was concerned solely with the pressure drop across the cavity, ours takes into account the losses in the nozzles and provides simple theoretical models to determine the overall pressure drop in the system. The models, which use solutions of the linear and nonlinear turbulent Ekman-layer equations, take account of the pressure drop in the cavity, of the mixing between the incoming fluid and that in the boundary layers and of the pressure drop inside the rotating nozzles. It is shown that, while the pressure drop in the cavity itself can be reduced to virtually zero, the overall pressure drop in the nozzles and the cavity always exceeds that associated with solid-body rotation.

The theoretical results were compared with experimental data obtained from a rotating-cavity rig with $x_a=0.5$, $0.02\leqslant|\lambda_T|\leqslant 0.5$, and $-0.4\leqslant c\leqslant+0.9$. The results obtained from the theoretical models were, in the main, in good agreement with the experimental data. For the cavity itself, the variation of $|C_w|$ with $C_{p,c}$ exhibited an "s-curve" characteristic with up to three values of $|C_w|$ for each value of $C_{p,c}$. However, when the pressure drop across the nozzles was included, the variation of $|C_w|$ with $C_{p,T}$ showed that the overall pressure drop was increased and that the "s curve" was attenuated to produce a virtually monotonic characteristic.

Acknowledgments

This research was conducted while the authors were at the

University of Sussex, and we wish to thank the Science and Engineering Research Council, Rolls Royce plc, and Ruston Gas Turbines Ltd for funding the work.

References

1 Chew, J. W., Farthing, P. R., Owen, J. M., and Stratford, B. The use of fins to reduce the pressure drop in a rotating cavity with radial inflow. *J. Turbomachinery*, 1989, **111**, 349–356

2 Farthing, P. R., Chew, J. W., and Owen, J. M. The use of de-swirl nozzles to reduce the pressure drop in a rotating cavity with radial inflow. ASME Paper 89-GT-184, 1989; *J. Turbomachinery*, to be published

3 Owen, J. M., Pincombe, J. R., and Robers, R. H. Source-sink flow inside a rotating cylindrical cavity. *J. Fluid Mech.*, 1985, **155**, 233–265

4 Owen, J. M. An approximate solution for the flow between a rotating and a stationary disc. *J. Turbomachinery*, 1989, **111**, 323–332

5 Owen, J. M. and Rogers, R. H. Flow and heat transfer in rotating-disc systems. Vol. 1, Rotor-stator systems. Research Studies Press, Taunton, UK, 1989

6 Karman, Th. von. Über laminare und turbulente Reibung. *Z. angew. Math. Mech.*, 1921, **1**, 233–252

7 Firouzian, M., Owen, J. M., Pincombe, J. R., and Rogers, R. H. Flow and heat transfer in a rotating cavity with a radial inflow of fluid. Part II: Velocity, pressure and heat transfer measurements. *Int. J. Heat and Fluid Flow*, 1986, **7**, 21–27

8 Batchelor, G. K. *An Introduction to Fluid Dynamics*. Cambridge University Press, 1967

9 Farthing, P. R. The effect of geometry on flow and heat transfer in a rotating cavity. D. Phil. thesis, University of Sussex, 1988